# Characteristics of radio frequency wave propagation in bounded plasma under the various magnetic field configurations

Shunjiro Shinohara[a] and Akira Fujii
*Interdisciplinary Graduate School of Engineering Sciences, Kyushu University, Kasuga, Fukuoka 816-8580, Japan*

(Received 29 August 2000; accepted 5 February 2001)

Detailed characteristics of radio frequency (rf) waves with pulsed modes in the whistler wave range were studied in a cylindrical rf-produced plasma, where the plasma boundary lay in the intermediate regime between infinite whistler wave propagation and bounded geometry helicon wave propagation. Excited magnetic field amplitudes and phases with three components in two-dimensional space were measured for different experimental conditions. Three magnetic field configurations were used and the diameter of the excitation loop antenna was also varied. Numerical calculation by the finite element method, which has been demonstrated to be a powerful means for this analysis, showed good agreement with the observed results, satisfying the dispersion relation and wave structures of helicons in the semisteady state and also satisfying the dispersion of whistlers with a short pulsed mode. The excited waves propagated nearly along the magnetic field lines within a small angle of less than 10°. Furthermore, in the low (high) collisionality regime, domination of standing (propagating) waves was found from the wave analysis. © *2001 American Institute of Physics.* [DOI: 10.1063/1.1368143]

## I. INTRODUCTION

A radio frequency (rf) wave with a frequency between ion and electron cyclotron frequencies, $f_{ci}$ and $f_{ce}$, respectively, is known as a whistler wave,[1,2] which has right-hand circular polarization. The spontaneous excitation of whistlers by lightning from the ionosphere was observed historically,[3,4] and this wave has been found to play important roles in the various space physics fields,[5] such as in the aurora ionosphere,[4,6] magnetotail,[7] and solar wind.[8] On the other hand, from knowledge of the character of this wave, probing of the entire plasmasphere can be performed by, for example, whistler spectrograms recorded on the ground.[9] As for basic laboratory research, which has some common and other different approaches from space plasma research (and thus both researches are complementary and important), detailed characterization of the whistler wave excited by several methods, such as the loop antennae, electrodes, and electron beams, and the role of the waves in these cases, have been clarified.[5,6,10–13]

One example of an application of the whistler wave is a helicon source.[14–18] The helicon wave is a bounded electromagnetic wave in the whistler wave range with both right- and left-hand circular polarization. This wave has been used for plasma generation in a high-density plasma source, which needs to have a large diameter in some cases.[19–21] In addition, an application to a magnetoplasma rocket[22] utilizing this wave has been proposed. Furthermore, there are a number of interesting phenomena involving this wave, such as a fast collisionless reconnection[23] and some types of turbulence[24] in the electron magnetohydrodynamic (EMHD) regime,[25] which describes the plasma behavior in the above frequency region on the scalelengths shorter than the ion skin depth $c/\omega_{pi}$ ($c$, velocity of light; $\omega_{pi}$, ion plasma angular frequency).

Although the fundamental wave characteristics of helicon waves are well known, there have been few detailed studies on the propagating characteristics of whistlers/helicons under the different magnetic field configurations in a limited boundary, nor have there been comparisons with the computation results in two-dimensional space. In whistlers, most of the experiments[10–13] have been performed so far under the conditions that the wave excited region along the radial direction was much smaller than the boundary size, using a small wave excitation source, which can be treated as an unbounded electromagnetic wave. Furthermore, wave packet excitation using a short pulse and measurement on the transient pulsed wave characteristics were done, which showed again approximately unbounded wave behavior along the axial direction. Wave studies under various field configurations for the case of a limited boundary (in our experiment, wave excited region is comparable to or slightly smaller than the boundary size) have been scarcely performed.

As for helicons,[15–17] which show a really bounded wave character, a high density plasma with small insulated tube radius less than 5 cm typically has been produced, using the antenna wound around the outer side of the insulation tube, in the straight magnetic field configurations. In our previous experiments,[15,19–21] we have made some studies about the production of a larger diameter plasma, for the condition of a larger metal boundary (side) than the wave excited region, and also some studies under different field geometries.[21,26–28] However, in those experiments, wave measurements were not done using the test wave, separating the source, which

[a]Electronic mail: sinohara@aees.kyushu-u.ac.jp

 

can be clearer for the wave characterization. In addition, an immersed antenna with the smaller radius than the metal wall radius (boundary effect is different from the insulating boundary) to excite the wave has not been tried for this test wave. Furthermore, reliable numerical calculations in the whole space (two dimensions) in whistlers/helicons have been scarcely reported, and no intensive and no direct comparative studies with the experiments to confirm the wave characteristics have been done, to our knowledge.

Thus, the study described here is very important for the understanding of wave characteristics for the case of a limited boundary between regions of unbounded whistlers and bounded helicons, and also to understand the characteristics under various magnetic field geometries. The comparison to the numerical results using a powerful code[29] to show the two-dimensional wave profiles also is important. Note that ray tracing calculations,[1,2] which have been sometimes employed in whistlers, cannot be applied in the present case, considering the ratio of the plasma size to the wavelength. The results obtained can be expected to contribute to the research fields mentioned above, such as the plasma processing field for optimum plasma production, the basic plasma and nuclear fusion fields for the plasma source (preionization and conditioning), and the space plasma field for the wave propagation in the complex magnetic field configurations. Here, we will briefly summarize the main results from the previous experiments[19,21,26–28] and the different points in order to show the objectives of the present study. Wave characteristics in two-dimensional space have been investigated for the cases of straight, divergent, convergent, and cusp magnetic fields. The excited wave was found to propagate nearly along the field, which is similar to the observation in the magnetotail.[7] The above experiments were performed to analyze the rf wave characteristics to understand the relationship between the density profile generated by this wave and the regions of the wave propagation and damping, for constructing a database so that a desired plasma profile can be generated. Therefore, the wave physics was blurred due to the plasma production during the wave propagation, which changed the plasma parameters. In addition, use of four-turn spiral antennae was not suitable from a viewpoint of the detailed wave studies, which should be performed using a wave excited by a local source.

The rf sources were separated into two, i.e., one was for plasma production and the other for the test wave propagating studies with a different rf frequency from the production one. In the research described in this paper, so that much clearer and more detailed results could be obtained. A local source, positioned in the plasma, was made as a single loop antenna, which was used to excite a test wave in an afterglow condition in order to reduce the noise. The radius of the loop could be changed. Boundary effects on the wave characteristics and wave structures were also considered from the viewpoint of whistlers/helicons and standing/propagating waves, as well as the phase and group velocities and propagation angle. The obtained results were compared directly and extensively to results computed using a finite element method (FEM),[29] which is a powerful tool for the interpretation of these results.

This paper is organized as follows. First, the experimental system and the computation procedure are described in Sec. II, followed by a brief theoretical background of whistlers/helicons in Sec. III. Next, contour plots of amplitude and the phase of the excited magnetic field in two-dimensional space under the three magnetic field configurations (straight, divergent, and convergent fields) are presented in Sec. IV. Good agreement between experimental and computation results was obtained, and the propagation characteristics including the wave structures and the standing wave formation are discussed. This contributed to the understanding of the wave physics in whistlers/helicons. Finally, Sec. V contains the conclusion.

## II. EXPERIMENTAL SETUP AND METHOD OF WAVE ANALYSIS

The experimental system[20,27] is shown in Fig. 1. Argon plasma at a filling pressure of $P=8-12$ mTorr was produced in a linear device, 45 cm in diameter, and 170 cm in axial length by a four-turn spiral antenna. The output rf power and frequency $f=\omega/2\pi$ were 2 kW (2 ms pulse with a duty of 1/11) and 7 MHz, respectively. A test rf wave was excited by two sizes of loop antennae, located at $z=10-15$ cm, with diameters of 10 and 30 cm (five turns each of copper wires with 0.1 cm diam) covered with the insulation material (0.5 cm thickness) to reduce the capacitive effects. Here, $z=0$ cm is defined as being at the window surface which faces the inner vacuum chamber. This test wave was excited in the afterglow phase with a pulse length of 1–50 $\mu$s, at the time of 0.3 ms after turning off the main rf power. At this time, the plasma density was about one-third of that produced by the main rf power pulse. Both rf systems have impedance matching boxes, directional couplers, and monitors of antenna currents and voltages to estimate the antenna characteristics and minimize the reflection loss.

Plasma parameters were measured by Langmuir probes, and typical results were electron density $n_e$ of $(0.5-1)\times10^{12}\,\mathrm{cm}^{-3}$ with electron temperature $T_e$ of 2–3 eV. The excited wave was detected by magnetic probes (two rotatable crossed probes, 0.5 cm in diameter), which were moved axially (continuous measuring positions) as well as radially

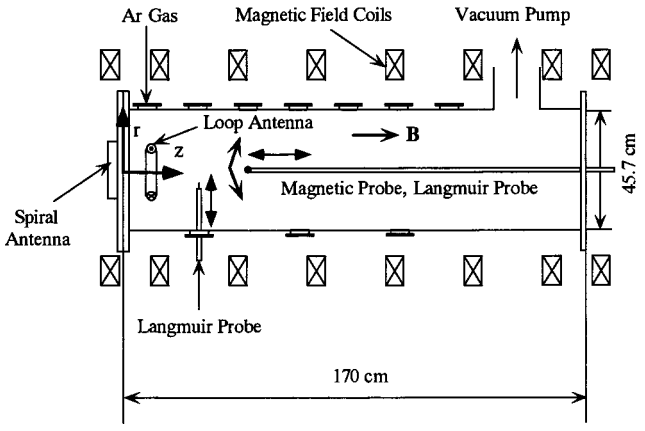


FIG. 1. Schematic view of the experimental device.

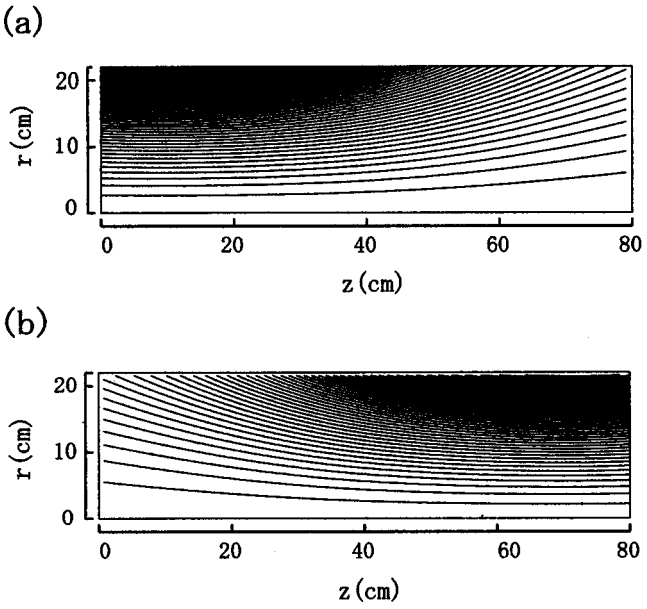


FIG. 2. Contour plots of the magnetic flux (linear scale) with (a) divergent and (b) convergent magnetic field configurations.

(seven positions typically) to pick up three components, $B_r$, $B_\theta$, and $B_z$ in the cylindrical geometry. Data were stored in a digital oscilloscope directly, and a boxcar integrator through a balanced mixer was used for the case of an interferometric measurement. With the use of a phase shifter, the amplitude and the phase of waves at each point could be estimated. In the present experiment, three magnetic field configurations were tested: uniform (magnetic field $B=40-60$ G), divergent [Fig. 2(a)] and convergent [Fig. 2(b)] fields. The magnetic field $B$ was ~54 (12) G at $z=0$ cm and ~8 (120) G at $z=80$ cm for the divergent (convergent) field case, and the angle between the field line and the $z$ axis at $z=80$ (0) cm and radius $r=10$ cm was ~9° for the divergent (convergent) field case.

Mostly, for the case of the antenna with 10 (30) cm diameter, uniform and divergent (convergent) fields were used with the test rf antenna current of 0.5–2 A with the input power less than 1 W. This power did not affect the plasma parameters, since it was three orders of magnitude lower than the rf production power. Here, the frequency $f$ of the test wave (=15 MHz) lay between two frequencies of $f_{ce}=22-340$ MHz (the effect of finite electron mass[17] mostly could be neglected) and $f_{ci}=0.3-5$ kHz satisfying the conditions of whistlers/helicons. Also, $f$ was larger than the lower hybrid frequency $f_{\mathrm{LH}}\sim\sqrt{f_{ce}f_{ci}}$ [the magnetic field range was also chosen as the reproducible plasma production by a spiral antenna with $f=7$ MHz (Ref. 20)]. The skin depth of $c/\omega_{pi}$ was 1.3–1.8 m, which was longer than the observed wavelengths by one order of magnitude. In our condition, electrons were magnetized and ions were unmagnetized (ion collides with ions and neutrals more than hundred times in one gyration time, while the estimated ion Larmor radius $r_{Li}$ was mostly less than the plasma radius $r_p$). These were similar to the condition in Ref. 10, except for the larger ratio of $r_{Li}$ to $r_p$. It should be noted that we observed excited waves in the various field configurations with a limited boundary under the semisteady state condition, except for the short pulse case, while Ref. 10 used mostly a single pulse with less than a 1 $\mu$s width only in the uniform magnetic field to see transient wave phenomena without the need of considering limited boundaries.

The Transport Analyzing System for tokamaK/Wave Analysis (TASK/WF) code was developed by Fukuyama,[29] using the FEM to solve vector and scalar potentials of the wave. This code analyzes wave propagation, using a linear treatment, in an inhomogeneous medium, in both two- and three-dimensional space, under various magnetic field configurations, plasma density profiles, antenna geometries, and boundary shapes. The response of the plasma is described by a cold-plasma dielectric tensor including collisions with neutrals. By the use of this advanced code, we can understand the experimentally obtained wave characteristics in this whistler frequency range with more detailed spatial structures, under the three magnetic field configurations with a limited boundary that were used in this study.

## III. BRIEF THEORETICAL BACKGROUND OF WHISTLERS/HELICONS

First, we will consider the dispersion relations of whistlers in unbounded boundaries. The phase and group velocities of $v_p$ and $v_g$, respectively, of the whistler wave propagating along the field lines can be written as follows,[2] using $n^2\sim\omega_{pe}^2/\omega\ \ \omega_{ce}$ as the approximate dispersion relation,

$$v_p=c\sqrt{\omega\omega_{ce}/\omega_{pe}^2}, \tag{1}$$

$$v_g=2v_p=2c\sqrt{\omega\omega_{ce}/\omega_{pe}^2}. \tag{2}$$

Here $n$ and $\omega_{pe}$ are the refractive index and the electron plasma angular frequency, respectively ($\omega_{ce}=f_{ce}/2\pi$). If the plane wave propagates (i.e., it has a phase velocity) obliquely with an angle of $\theta$ with respect to the magnetic field, a factor of $\sqrt{\cos\theta}$ must be multiplied in both of Eqs. (1) and (2) for velocities along the field lines. From these equations, both $v_p$ and $v_g$ increase with $\sqrt{\omega}$ (i.e., they have dispersive characters), and for the case that the wave propagates not along the field line, the expressions for $v_p$ and $v_g$ become the same as those in the following helicon wave case, respectively, although for helicons, the perpendicular wave number $T$ is determined by the boundary condition, not by the excitation wave angle determined by the antenna (this will be described later in this section). In our experiment, errors in using Eqs. (1) and (2) were small, even in the low field region where $\omega$ was approaching $\omega_{ce}$ (typically less than 20%), and the curvature effect of the magnetic field was considered to be small, since the wave propagated nearly along the field lines, as shown in the experimental results described later.

Note that, for this plane whistler wave, theoretically,[2] $\theta_g$ (the propagation angle between $v_g$ and $B$) increases with $\theta_p$ (propagation angle between $v_p$ and $B$) and becomes maximum at the critical angle of $\theta_c=19.5°$ at $\theta_p=54.7°$, and then $\theta_g$ decreases with further increase in $\theta_p$. In other words, regardless of the value of $\theta_p$, the wave energy flows

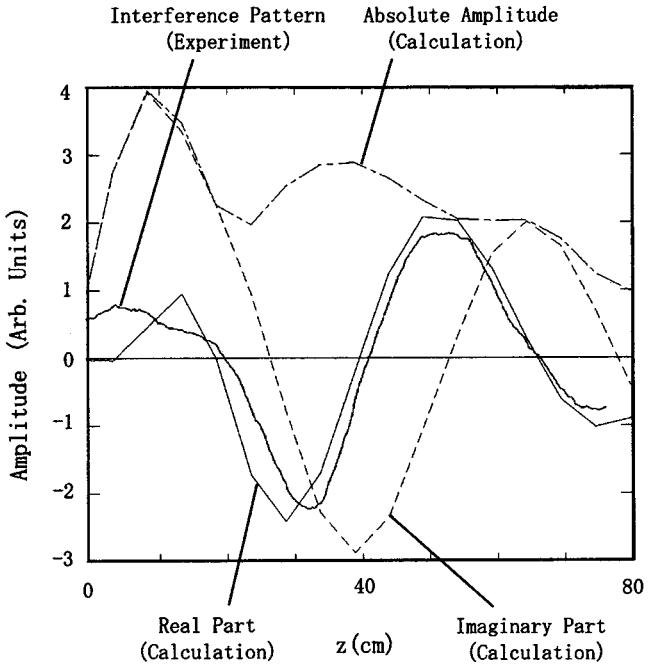


FIG. 3. Comparison of axial profiles of $B_z$ on axis between experiment and computation, for the case of a uniform magnetic field ($B=42$ G) and a $\phi$ 30 cm antenna.

within a cone angle of $\theta_c$. This critical angle is dependent on several parameters[30,31] but does not change appreciably from 19.5° in our experimental conditions. It is known as that the most of the wave energy propagates with a localized cone angle of $\theta_r$ with respect to the external magnetic field. This is known as the resonance cone.[31] This angle was solved for the potential of an oscillating point charge,[32] and in our experimental conditions of $f_{pe}$ (electron plasma frequency) $\gg f_{ce}$, this cone angle can be expressed approximately as $\sim\sin^{-1}(\omega/\omega_{ce})$, which was typically small, of the order of several degrees, for our conditions of $\omega_{ce}\gg\omega$, although we did not use a small source without boundaries.

Next, we will describe helicon wave characteristics. In our previous experiments,[20] a helicon wave with azimuthal mode number of $m=0$ was excited using a spiral antenna, while in the present paper, a loop type antenna is expected to excite the $m=0$ mode. For the case of a uniform density profile,[18] wave fields with $m=0$ are expressed as Bessel functions of $J_n$: both $B_r$ and $B_\theta$ are proportional to $J_1(Tr)$, and $B_z$ to $J_0(Tr)$, where the perpendicular wave number $T$ is $3.8/a$ for the case of the lowest radial mode, where $a$ is the effective radius. In this case, $B_z$ peaks on axis and both $B_r$ and $B_\theta$ peak at $r/a=0.48$, while $B_z$ (both $B_r$ and $B_\theta$) becomes zero when $r/a$ is 0.63 (0 and 1). Normally $a$ can be taken as the inner radius of the insulated discharge tube because of the character of the helicon wave imposed by the boundary, except for a few cases[20] including the present experiment that there are roughly two regions with and without the dominant helicon wave propagation in the radial direction.

Using the relation[18] of $T^2=\alpha^2-k^2$ ($k$ is the parallel

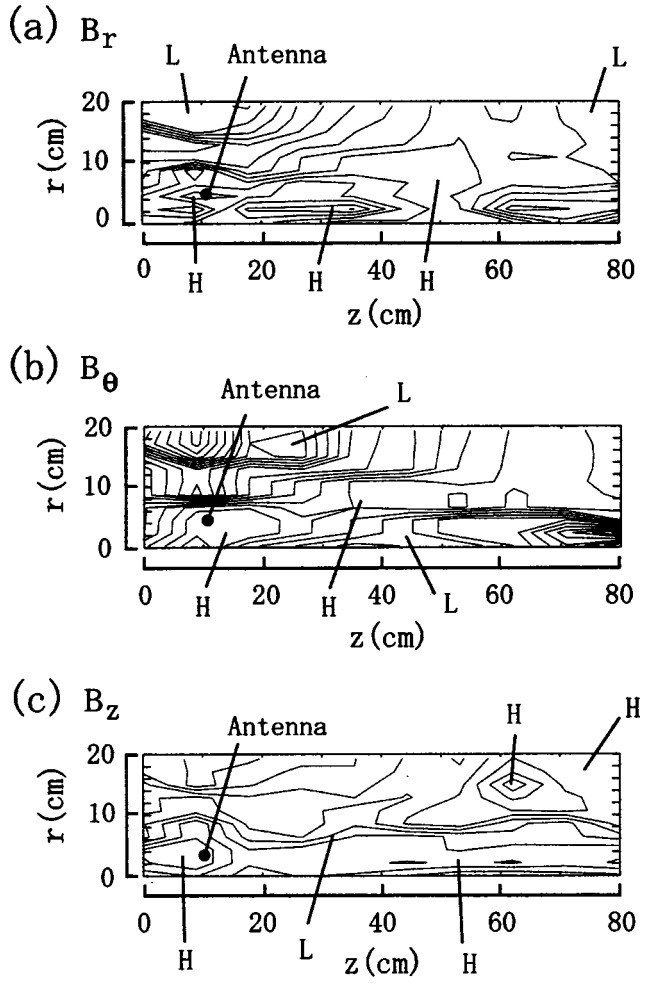


FIG. 4. Contour plots (logarithmic scale) of amplitude of (a) $B_r$, (b) $B_\theta$, and (c) $B_z$, for the case of a uniform magnetic field ($B=60$ G) and a $\phi$ 10 cm antenna (experiment). Here, $H$ and $L$ denote the higher and the lower amplitudes, respectively, compared with those in the neighboring regions.

wave number) with $\alpha=(\omega/k)$ $(\omega_{pe}^2/\omega_{ce}c^2)$, $v_p$ and $v_g$ along the field line direction are expressed as follows:

$$v_p=(\omega_{ce}c^2/\omega_{pe}^2)\sqrt{k^2+T^2}=\omega/k, \tag{3}$$

$$v_g=(\omega_{ce}c^2/\omega_{pe}^2)^2(k/\omega)(2k^2+T^2). \tag{4}$$

Here, $k$ can be written as

$$k^2=(1/2)\{-T^2+\sqrt{T^4+4[(\omega\omega_{pe}^2/\omega_{ce}c^2)^2]}\}. \tag{5}$$

## IV. COMPARISON BETWEEN EXPERIMENTAL AND COMPUTATION RESULTS

The wave characteristics of the experiment and the computation were compared in detail, typically, in the form of contour maps in two-dimensional geometry. Before doing this, we checked the wave patterns as a function of the $z$ axis in the uniform field. The results are shown in Fig. 3. The interference wave pattern obtained experimentally was in good agreement with the real part of the computation pattern for the case of parallel wavelength $\lambda$ of ~50 cm. In the computation, the mesh interval was 2 cm in both the radial and the axial directions, and results were not different appreciably from those for the case of 1 cm interval in both direc-

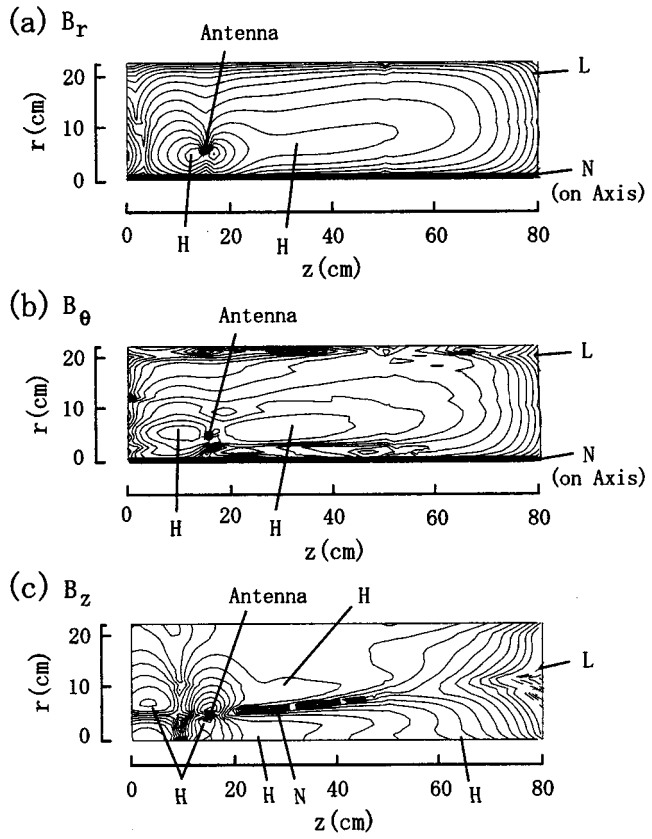


FIG. 5. Contour plots (logarithmic scale) of amplitude of (a) $B_r$, (b) $B_\theta$, and (c) $B_z$, for the same condition as that in Fig. 4 (computation). Here, $N$ denotes the zero value (node) in a linear scale, i.e., zero amplitude.

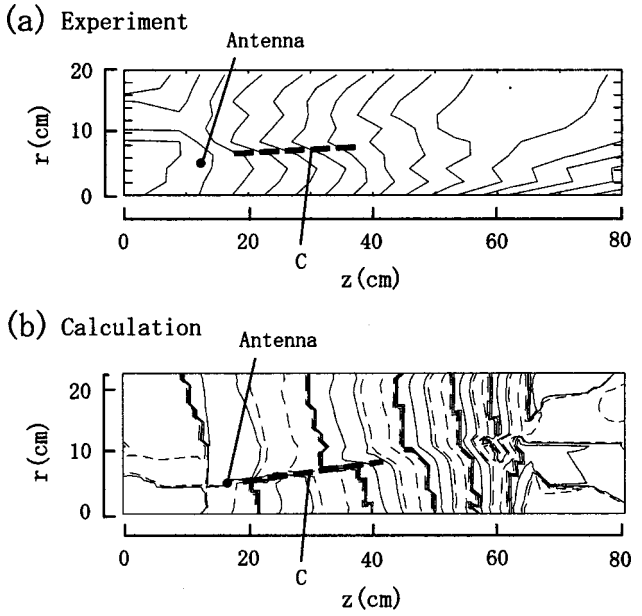


FIG. 6. Contour plots (linear scale) of phase of $B_z$ from (a) experiment and (b) computation, for the same condition as that in Fig. 4. Here, $C$ denotes the phase change of $\pi$, i.e., the polarity change of amplitude in a linear scale.

tions. Needless to say, depending on phase (or time), wave structures change between the forms given by the real and imaginary parts of the wave computed in the simulation. In addition to the present case, in which agreement of the amplitude and the phase change in two-dimensional space was found, and other cases, such as the divergent field case, the feasibility of this code was confirmed previously for different magnetic field configurations (divergent, convergent, and cusp magnetic field configurations[27,28]).

Hereafter, we will show the results in the following order: cases under (1) uniform, (2) divergent, and (3) convergent magnetic fields, followed by the cases of (4) a short pulse and a standing wave. Except for the short pulse case, the excited wave was analyzed with the semisteady state with a pulse length of $<50$ $\mu$s. First, the uniform field case ($B=60$ G) with the antenna diameter of 10 cm is presented for wave analysis. Note that the plasma extended to the inner wall surface and the ratio $R$ of the wall radius to the antenna radius was 4.5. Figure 4 shows two-dimensional (spatial) contour plots of the amplitude of magnetic field, $B_r$, $B_\theta$, and $B_z$, in the experiment. Here, the intervals between the contour lines in the logarithmic scale was 0.2, and symbols of $H$ and $L$ denote the higher and the lower amplitudes, respectively, compared with those in the neighboring regions. This constant scale value and symbols were used throughout this paper. It can be seen that the amplitudes of $B_r$ and $B_\theta$ were larger away from the axis while that of $B_z$ was larger near the central axis (see $H$ regions), and the phase of $B_z$ at $z<40$ cm changed by $\sim\pi$ radians in the radial direction from the central axis to the wall, i.e., polarity change. This can be seen in Fig. 6(a) below, shown by the thick dotted line at $r=7-8$ cm. Although the radial resolution was not so good due to, typically, seven radial measuring positions mentioned before, these characteristics are similar with that of the theoretical wave structure of the helicon wave[14,18,20] with $m=0$, which was described in Sec. III.

As shown in Fig. 5, the computation results for the same condition as the results shown in Fig. 4 were consistent with the experimental ones, and showed clearer phenomena of wave propagation than those in the experiment (see regions at $r=0-10$ cm and $z=10-40$ cm and also $H$ regions). In this figure, $N$ denotes the zero value (node) in a linear scale meaning throughout this paper: zero amplitudes on $r=0$ for $B_r$ and $B_\theta$, and $r=5-7$ cm ($z$ is around 20–40 cm) for $B_z$. It can be seen again that amplitudes of $B_r$ and $B_\theta$ were larger away from the axis, while that of $B_z$ was larger near the central axis and increased again along the radial direction after crossing the zero amplitude zone (the thick dotted line denoted as $N$).

Figure 6 shows contour plots of the phase of $B_z$ in the linear scale (all intervals in this paper are $\pi/2$ radians) in both of the experiment and the computation. Here, in the calculation, solid (dotted) lines show the positive (negative) values and four nearly overlapping lines denote a phase jump of 2 $\pi$ radians due to the periodicity (phases were defined within the region of $-\pi$ to $\pi$ radians). Good agreement was observed for the region $z<40$ cm including the $\pi$ phase change position, i.e., the polarity changes at $r=5-7$ cm denoted as thick dashed lines and the symbol $C$, which corresponds to $N$ in Fig. 5(c). However, the agreement became poor in the region further away from the antenna mainly due to the poor radial resolution and lower amplitude (low signal

to noise ratio) in this region. The effect of the different density profiles must also be considered, since we did not have fully two-dimensional data of plasma parameters. Generally, the density became lower toward the edge in the $r$ and $z$ directions in the experiment, while a uniform density profile was assumed in the calculation.

Although slightly divergent wave propagation patterns in the radial direction with $z$ can be seen in Figs. 4–6, the spread angle with respect to the straight magnetic field direction for the experiment (computation) was within 5° (10°), which was smaller than the critical angle $\theta_c$ of 19.5° and was comparable to the resonance cone $\theta_r \sim 5°$ in this straight field case of $B=60$ G. Those two angles can be defined for the whistlers, as discussed in Sec. III, although neither a very small source compared to the plasma region, nor a transient short pulse were used in our experiment. On the other hand, for the helicon waves, the phase signals show the parallel velocity and parallel wavelength without the perpendicular components. Standing wave patterns are formed in the radial (perpendicular) direction, which are consistent with the theoretical expectation of parallel wave propagation (group velocity) in the uniform magnetic field.[18]

From Fig. 6, λ was estimated to be ~20 cm at $z=30$ cm, which corresponds to $v_p \sim 3\times10^6$ m/s. These values were consistent with those of whistlers [$\sim 1.8\times10^6$ m/s from Eq. (1)] and the helicon waves [$\sim 3\times10^6$ and $\sim 2.1\times10^6$ m/s from Eq. (3) with $a=5$ cm ($T=0.76\,\mathrm{cm}^{-1}$) and $a=10$ cm ($T=0.38\,\mathrm{cm}^{-1}$), respectively]. Note that values of $k$ were not the same in the evaluation of the above velocities. The increasing wavelength in the region further away from the antenna ($z>40$ cm) is mainly due to the decrease in the density [see e.g., Eq. (1)]. In our experiments, the phase velocities between whistlers and the helicon waves are not so much different, due to the use of the larger vacuum vessel (smaller $T$ value) compared with the case normally used in a helicon source, which has a larger $T$ value due to the smaller plasma radius. It should be noted that the Alfvén velocity was slower than the whistler velocity in our experiment by two orders of magnitude.

The observed characters in Figs. 4–6, in sum, indicate a helicon wave character with nearly parallel propagation (slightly oblique propagation) instead of that of whistlers from the observed wave structures, especially the Bessel function like radial structures, although there was not an appreciable difference of the phase velocities under our experimental conditions. The striking point is that even though the radius of the excitation loop antenna immersed in the plasma is smaller than the inner radius of the vacuum chamber (the ratio $R$ between two radii was 4.5), which is made of stainless steel, the helicon wave could be excited to propagate first in the test wave excitation with two different regions; the inner radial region where the most of the wave energy was concentrated and the outer region where wave energy was small. This is seen in Figs. 5 and 6, in that the radii of thick dashed lines in the $B_z$ signals denoted as $N$ and $C$ were smaller than the chamber radius by less than one third. This feature has not been found, as far as we know, except for our previous work[19,20] under different experimental conditions. In the previous work, an excitation loop with a larger size, located outside the chamber at the end section through an insulation window, was used for plasma production but not as a test wave generator. Note that in most past experiments done so far, as we mentioned before, antennas were wound around the outside of a small insulation tube, and the waves excited in the whole plasma region extended to the inner wall radius.

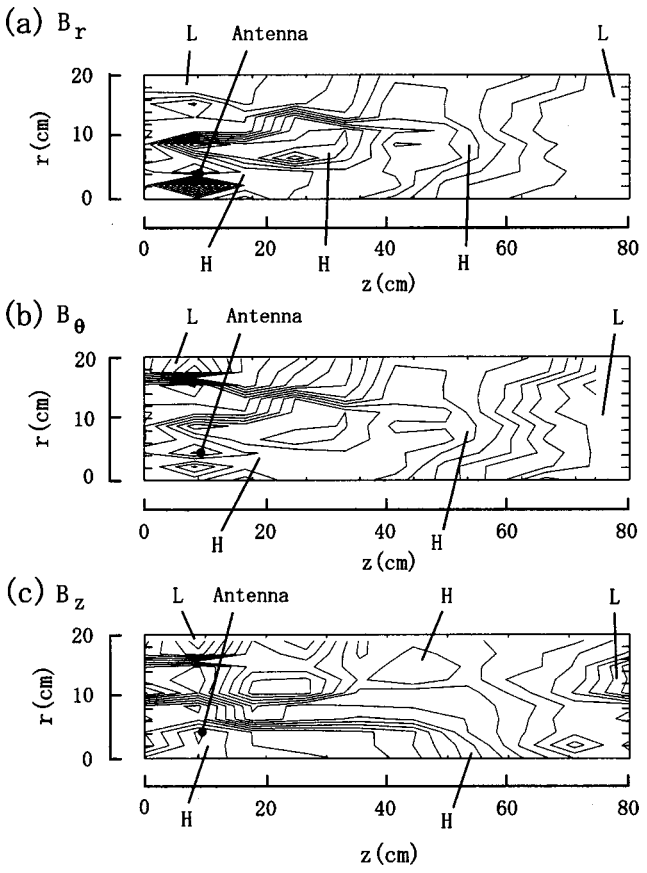


FIG. 7. Contour plots (logarithmic scale) of amplitude of (a) $B_r$, (b) $B_\theta$, and (c) $B_z$, for the case of a divergent magnetic field and a $\phi$ 10 cm antenna (experiment).

Next, the results for the divergent field case, shown in Fig. 2(a), are presented. Figure 7 shows two-dimensional contour plots of the amplitude of magnetic field (three components) for the experiment, performed with the antenna diameter of 10 cm. Compared with the uniform field case in Fig. 4, the excited fields spread more radially (a slight effect is due to the weak divergent field curvature) with an advance in the $z$ position. On the surface, the smaller damping length along the axis direction was found to be due to the geometrical effect of the divergent field, which is in contrast with the case of the convergent field (Fig. 9 below). The magnetic field line touching the antenna at a radius of $r=5$ cm lies at $r\sim13$ cm on $z=80$ cm in Fig. 2(a), which was consistent with the lower amplitude region of $B_z$ experimentally observed and shown in Fig. 7(c). In other words, the trench boundary between regions having positive and negative $B_z$ values (see the phase discussion below) diverged slightly with $z$. This means that the wave propagated (wave energy) nearly along the curved field lines (within 5°), which was

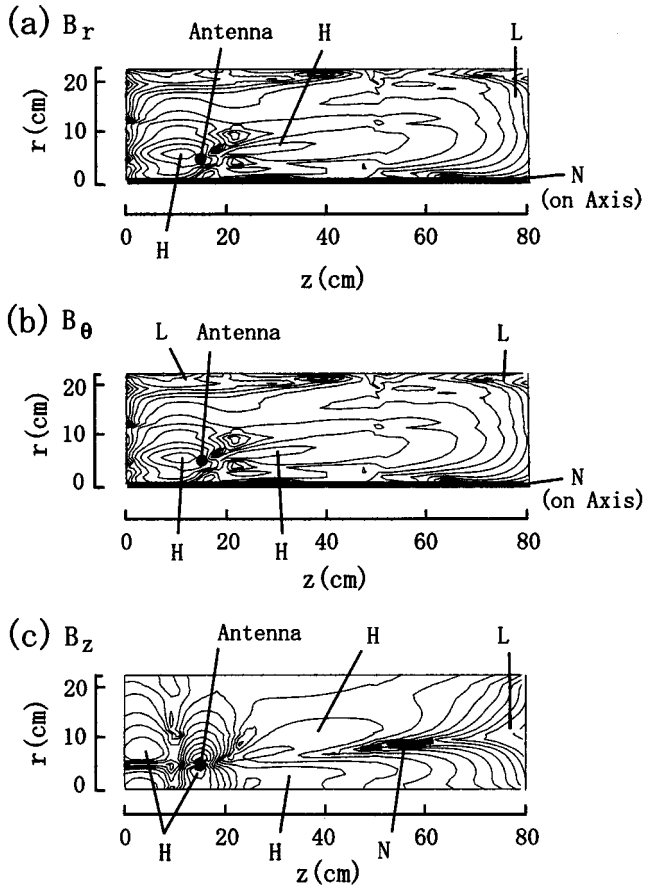


FIG. 8. Contour plots (logarithmic scale) of amplitude of (a) $B_r$, (b) $B_\theta$, and (c) $B_z$, for the same condition as that in Fig. 7 (computation).

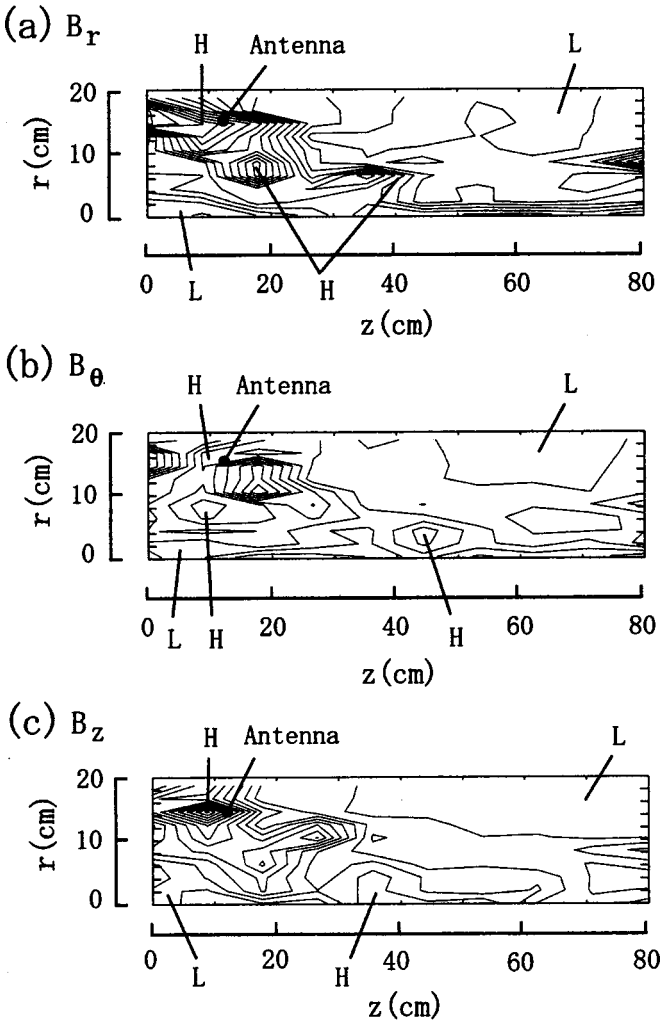


FIG. 9. Contour plots (logarithmic scale) of amplitude of (a) $B_r$, (b) $B_\theta$, and (c) $B_z$, for the case of a convergent magnetic field and a $\phi$ 30 cm antenna (experiment).

again consistent with the character of whistlers/helicons. The trend of this spread was supported by the computation, which showed the phenomena more clearly, as is shown in Fig. 8. This can be seen by comparing the $H$ regions for $z<40$ cm with the $L$ regions at $z\sim75$ cm.

At a fixed $z$ position, phases changed by $\sim\pi$ radians (near the radius comparable to the antenna radius) in the radial direction from the central axis to the wall in both of the experiment and computation (not shown), and the wavelength became shorter with $z$ due to the decrease in the magnetic field strength from the dispersion relation, as indicated by Eq. (1). Here, $\lambda$ was $\sim$13 cm at $z=30$ cm, corresponding to $v_p\sim2\times10^6$ m/s. This value was consistent with those of whistlers [$\sim1.5\times10^6$ m/s from Eq. (1)] and the helicon waves [ $\sim2.2\times10^6$ and $\sim1.7\times10^6$ m/s from Eq. (3) with $a=5$ and 10 cm, respectively]. The obtained data for this magnetic field configuration again indicated helicon wave structures with nearly parallel propagation along the field lines.

Third, we present the results for the convergent field, shown in Fig. 2(b). In contrast to the above case of the divergent field, a radial shrinkage of the wave excited region (all three components of the magnetic fields) along the radial direction was very clearly observed. Figure 9 shows two-dimensional contour plots for this experiment, performed with the antenna diameter of 30 cm (the ratio $R$ was 1.5). This result could be simulated by the computation in Fig. 10 very well (see $H$ regions with $z<50$ cm), showing that the wave propagated nearly along the curved field lines (within 10°). There was a tendency that the deviation angle from the field lines in the computation was slightly larger than that in the experiment. This shrinkage was also confirmed from the phase analysis in both of the experiment and the computation (not shown). The phase changed in the radial direction by $\sim\pi$ radians at $r<6$ cm ($z<30$ cm), and the position of this change decreased with an advance in $z$. However, $B_z$ components in both experiment and computation did not peak on axis, especially near the antenna region, and they have similar structures with the $B_r$ and $B_\theta$ components, which were different from the helicon wave structure of $m=0$ mode. This may come from the smaller ratio of $R$ (metal boundary effect was large) and the weaker magnetic field near the antenna region ($\sim$20 G). From the phase analysis, $\lambda$ was $\sim$17 cm at $z=30$ cm, corresponding to $v_p\sim2.6\times10^6$ m/s. These values were consistent again with those of whistlers ($\sim1.5\times10^6$ m/s) and the helicon waves ($\sim2.2\times10^6$ and $\sim1.7\times10^6$ m/s with $a=5$ and 10 cm, respectively). The slight increase in $\lambda$ as a function of $z$ ($z<50$ cm) could be under-

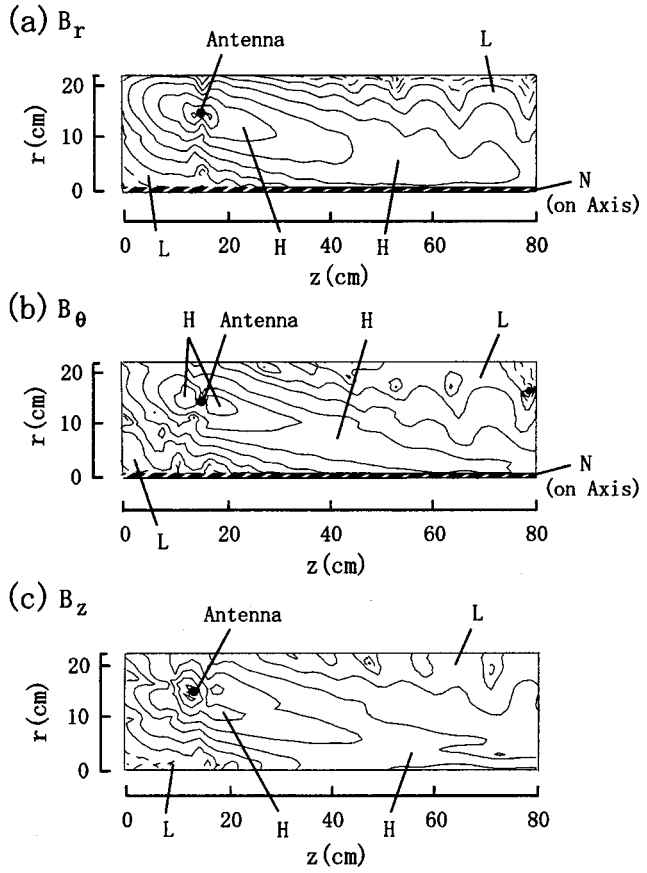


FIG. 10. Contour plots (logarithmic scale) of amplitude of (a) $B_r$, (b) $B_\theta$, and (c) $B_z$, for the same condition as that in Fig. 9 (computation).

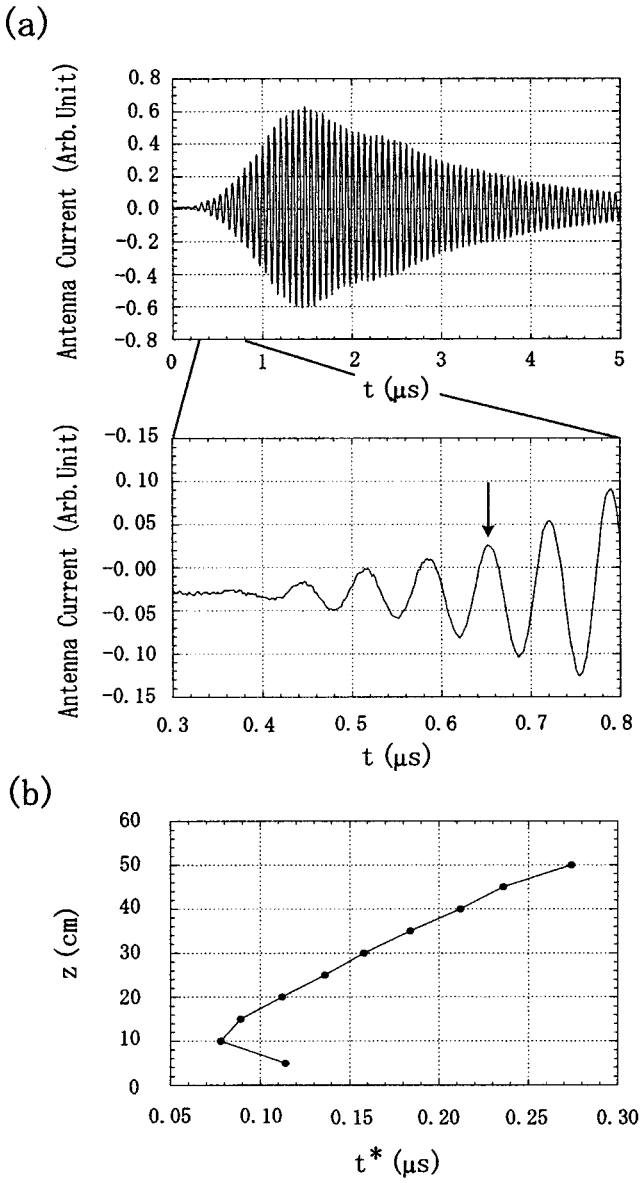


FIG. 11. (a) Time evolution of antenna current and (b) position of the $B_z$ component (the fourth wave) as a function of time, for the case of a divergent magnetic field and a $\phi$ 10 cm antenna (experiment). Here, $t^*$ was shifted compared with $t$ by $\sim 0.6$ $\mu$s.

stood as the increase in the magnetic field from the dispersion again.

Finally, the result for the short pulse case and the domination of the standing wave phenomena are presented. In order to see the time behavior of the wave propagation as well as to estimate the $v_g$ value instead of $v_p$, a short pulse with a length of $\sim 5$ $\mu$s was excited, as shown in Fig. 11(a). The main excited antenna frequency, determined from the Fourier spectrum was 15 MHz, with additional components at, e.g., 30 and 45 MHz with lower amplitudes. The obtained magnetic signals showed the main frequency of 15 MHz with the smaller amplitudes with frequencies of 5, 30, and 45 MHz, having amplitudes much less than 10% of the main component. The amplitude ratio of the main frequency to that of the other frequencies changed from position to position. By tracking the movement of a position of the fourth peak of the wave amplitude, $B_z$ component, as shown in the lower part of Fig. 11(a), the group velocity of the wave was estimated. In this case, the wave was excited by a loop antenna with 10 cm diam (current was $\sim 0.1$ A and power was less than 0.01 W) in the divergent field, and there was no appreciable qualitative difference of the pulse propagating character between the cases in the uniform and the divergent fields. In addition, other peaks, such as the first and the second peaks in the pulse train have the same results as the fourth peak case.

From Fig. 11(b), this peak moved in both positive and negative $z$ directions ($t^*$ was shifted compared with $t$ by $\sim 0.6$ $\mu$s) due to the nondirectivity radiation compared with the good directivity by a linked loop-torus antenna.[13] Here, the measurements were done at $r=0$ cm, changing the $z$ position. The speed of $v_g$ in the positive $z$ direction was almost constant at $\sim 2\times 10^6$ m/s in the period of $t^*=0.1-0.25$ $\mu$s, excluding the initial time of $t<0.1$ $\mu$s, since near the antenna (in other words, $t<0.1$ $\mu$s) the geometrical effect of the antenna must be considered. Effects of the oblique propagation and the field curvature on the propagating characters were also considered to be relatively small at $t>0.1$ $\mu$s (see the results in the divergent field mentioned before). The $v_g$ value obtained in this way was consistent again with those of whistlers [$\sim 2.8\times 10^6$ m/s from Eq. (2)] and helicon waves [$\sim 2.1\times 10^6$ and $\sim 2.0\times 10^6$ m/s with $a=5$ and 10 cm, re-

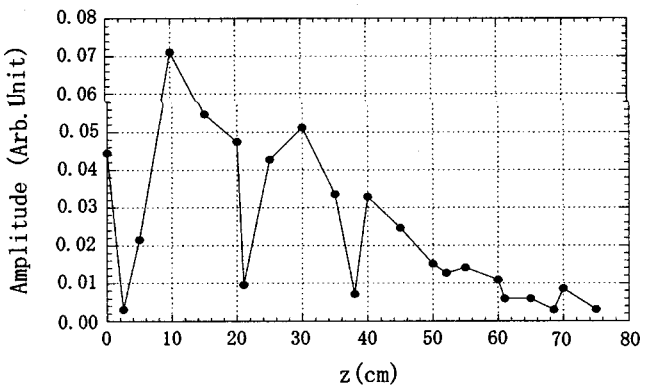


FIG. 12. Axial profile of the maximum amplitude of $B_z$ on axis, for the case of a divergent magnetic field and a $\phi$ 10 cm antenna (experiment).

spectively, from Eq. (4)]. In this initial pulse phase when the wave trains did not reach the boundary, the helicon wave can be excluded as a candidate of the excited wave, because the helicons need the boundary condition to have a $T$ value after reflecting from the boundary. Even if the pulses of the first, the second, and the third peaks can affect the propagation of the fourth peak, this effect is considered to be negligible because their amplitudes were smaller than the observed amplitude of the fourth peak [see Fig. 11(a)] for our conditions. In addition, the observed transient wave did not show helicon wave structures, e.g., similar to the Bessel function profiles. Therefore, the observed pulses are considered to have the features of whistlers, under the finite value of $R=4.5$.

In the experiment presented above, the normalized collision $\nu^*=\nu/\omega$ was mostly above 0.3, which excluded the presence of dominant standing waves. Here, $\nu$ is the sum of electron–neutrals and electron–ion Coulomb collisions, with the former collision being more frequent than the latter for our experimental conditions. Figure 12 shows an example of a standing wave pattern mixed with the propagating wave observed in the divergent field with 10 cm antenna radius, reducing $\nu^*$ to $\sim$0.2. This same wave feature was also found in the uniform field. Here, the maximum amplitude of $B_z$ in the several tens of rf periods was plotted as a function of $z$. Amplitude dips like nodes were observed at $z=20$ and 40 cm, which showed $v_p \sim 6\times 10^6$ m/s (this value was consistent with the estimation of $v_p$ for whistlers and helicons), where $\lambda$ was estimated to be twice the distance between the neighboring dips. This standing wave pattern was verified qualitatively in the computation (Fig. 13), changing $\nu^*$ from 0.1 to 0.5 through 0.2, with the same experimental condition as in Fig. 12 except for the collision parameter of $\nu^*$. From this figure, especially from the profiles of the absolute amplitude, the standing wave pattern can be seen. It was clearly observed with the low $\nu^*$ value of 0.1, weakened with increasing $\nu^*$ and disappeared almost completely at $\nu^*=0.5$. The observed phenomena of the mixture of the standing and propagating waves may be mainly understood from the boundary effects in the axial and radial directions, but nonmonochromatic wave excitation and the near field effect may also be important factors. In the axial direction, the ratio of the damping length $\lambda_d$ to the chamber size $L$ along the $z$ direction can be a parameter. For the case of $\nu^*=0.2$, this damping length[18] in our condition was estimated to be $\sim$0.6 m, which is comparable to the effective size $L$ along the $z$ direction. Increasing $\nu^*$ makes $\lambda_d$ shorter inversely, and the smaller value of $\lambda_d/L$ contributes the weaker effect on the standing wave formation.

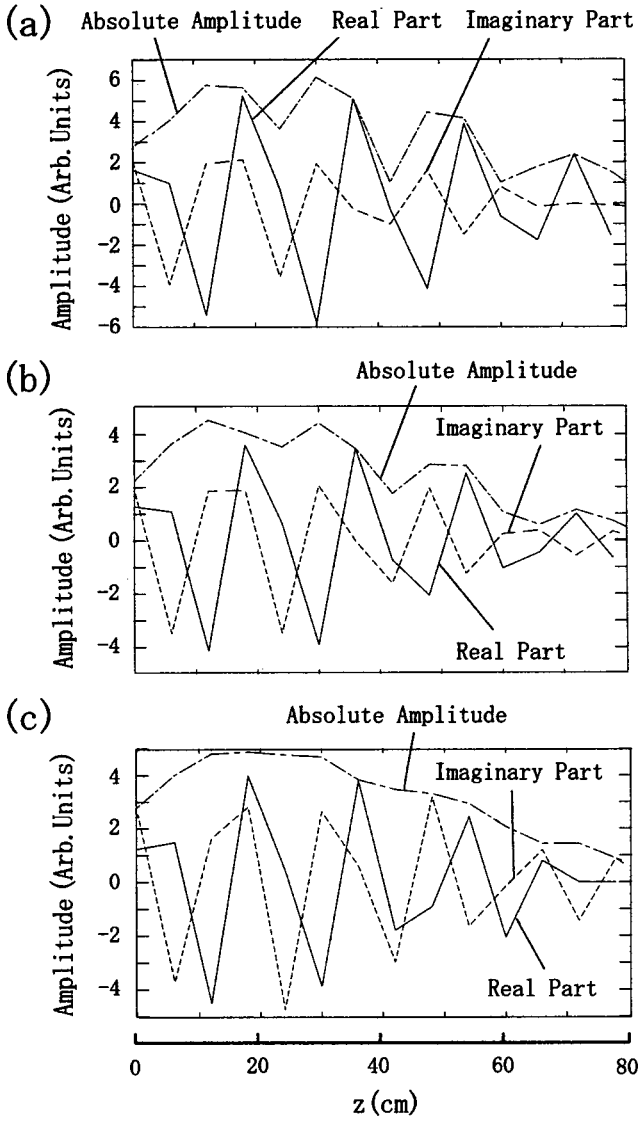


FIG. 13. Axial profile of amplitude of $B_z$ on axis, changing normalized collision frequency $\nu^*=\nu/\omega$ as (a) 0.1, (b) 0.2, and (c) 0.5, for the case of a uniform magnetic field and a $\phi$ 10 cm antenna (computation).

From the various results for semicontinuous wave excitation described above in which the ratio $R$ was 1.5–4.5, it can be concluded that the excited waves exhibited the character of helicons rather than whistlers in the helicon plasma source,[20] whose radius was larger than this type of sources normally used. This can be concluded even though the values of $v_p$ experimentally obtained were in good agreement with the dispersions of helicons and whistlers within a factor of 1.5. This conclusion came from the fact that we observed a ''standing wavelike character'' of the excited magnetic fields in the radial direction (e.g., in the helicon source, as was mentioned, a Bessel function radial profile is expected in

the uniform density case[18]), and the collision was relatively high to avoid a strong boundary (vacuum chamber) effect in the axial direction, which was discussed above.

It should be remembered that expressions of $v_p$ and $v_g$ for the whistler wave are the same as those of the helicon wave if both waves have the same $k$ and $T$ values, but the $T$ can be changed arbitrary for whistlers by the excitation antenna geometry, and for helicons by the boundaries. In other words, we can say that the observed waves were formed as the mixtures of incoming and reflecting whistler waves (to have helicon wave types) affected by the boundaries.[6] Note that, in the present case, boundaries (main wave excited region) were determined by the antenna radius (and thus the value of $T$ was determined by this radius),[20] but not by the chamber or the plasma radius, which is normally important.[18] As for the group velocity, from the short pulse experiment, $v_g$ was found to obey the whistlers derived from the dispersion, because the boundaries could not play an role in the pulse phase (wave packets) in contrast to the semicontinuous waves.

The propagation angles with respect to the field lines derived from the plots of the amplitude and phases, which included the information of the phase and group velocities, were much less than $\theta_c = 19.5°$ (and were not more than the typical resonance cone angle of $\theta_r$) for the three magnetic field configurations. The above results in the test wave experiment case, where the input rf power was less than 1 W, could be understood by the linear wave analysis.

From the knowledge obtained from these results, in addition to the contribution to the space plasmas under the various field topologies, the following considerations are necessary in order to construct an optimized scheme for a plasma production source. In the whistler wave range, the wave energy, whose region and wavenumbers can be determined by the antenna geometry and the wave dispersion, is carried nearly along the field, and boundary effect was important even the excitation antenna size is small compared to the device size. Therefore, for plasma production in this regime, we can list up the important factors as magnetic field configuration (rf plasma production in the cusp field,[21,26,27] in which rf wave characteristics was not treated in the present paper, is also attractive for good uniformity of the plasma density distribution), antenna design (induced capacitive field[14] also should be minimized), effect of a standing wave formation determined by the damping length and the device size in the axial as well as the radial directions, and diffusion along and across the field lines.[3]

## V. CONCLUSIONS

Detailed characteristics of rf waves with pulsed modes in the whistler wave range were studied in a cylindrical rf-produced plasma, where the boundary lay in the intermediate regime between infinite whistler wave propagation and bounded geometry helicon wave propagation. Excited magnetic field amplitudes and phases with three components in two-dimensional space were measured for different experimental conditions. Three magnetic field configurations (straight, divergent, and convergent fields) were used and the diameter of the excitation loop antenna (10 and 30 cm, where the ratios $R$ were 4.5 and 1.5, respectively), in the afterglow cylindrical plasma was also varied.

Numerical calculation by the finite element method, using the TASK/WF code, which has been demonstrated to be a powerful and effective means for this analysis, showed good agreement with the experimental results. The observed waves satisfied the dispersion relation of whistlers/helicons and wave structures (Bessel function like behaviors) of helicons: the semisteady state test wave except for the convergent field case with a small ratio of $R$ showed characters of helicons, while the short pulsed mode (packet) showed those of whistlers. The excited waves were found to propagate nearly along the magnetic field lines within an small angle of 10°, which was less than that of $\theta_c = 19.5°$ and was not larger than $\theta_r$. It was also found that in the low (high) collisionality regime, in which the boundary was $\nu/\omega$ was around 0.2 in our condition, standing (propagating) waves were dominant from the wave analysis.

## ACKNOWLEDGMENTS

We would like to thank Professor A. Fukuyama for the use of the TASK/WF code, Professor Y. Kawai for his continuous encouragement, and Dr. M. D. Bowden for checking the English.

[1] T. H. Stix, *Waves in Plasmas* (American Institute of Physics, New York, 1992).
[2] D. G. Swanson, *Plasma Waves* (Academic, San Diego, 1989).
[3] F. F. Chen, *Introduction to Plasma Physics and Controlled Fusion* (Plenum, New York, 1990).
[4] *Plasma Physics: An Introductory Course*, edited by R. Dendy (Cambridge University Press, New York, 1993).
[5] R. L. Stenzel, J. Geophys. Res., [Oceans] **104**, 14379 (1999).
[6] J. E. Maggs, G. J. Morales, and W. Gekelman, Phys. Plasmas **4**, 1881 (1997).
[7] Y. Zhang, L. H. Matsumoto, and H. Kojima, J. Geophys. Res., [Oceans] **104**, 28633 (1999).
[8] N. Lin, P. J. Kellogg, R. J. MacDowall, E. E. Scime, A. Balogh, R. J. Forsyth, D. J. McComas, and J. L. Phillips, J. Geophys. Res., [Oceans] **103**, 12023 (1998).
[9] R. P. Singh, A. K. Singh, and D. K. Singh, J. Atmos. Sol.-Terr. Phys. **60**, 495 (1998).
[10] R. L. Stenzel, J. M. Urrutia, and C. L. Rousculp, Phys. Fluids B **5**, 325 (1993).
[11] J. M. Urrutia, R. L. Stenzel, and C. L. Rousculp, Phys. Plasmas **1**, 1432 (1994).
[12] C. Krafft, P. Thévenet, G. Matthieussent, B. Lundin, G. Belmont, B. Lembège, J. Solomon, J. Lavergnat, and T. Lehner, Phys. Rev. Lett. **72**, 649 (1994).
[13] R. L. Stenzel and J. M. Urrutia, Phys. Plasmas **6**, 2989 (1999).
[14] M. A. Lieberman and A. J. Lichtenberg, *Principles of Plasma Discharges and Materials Processing* (Wiley, New York, 1994).
[15] S. Shinohara, Jpn. J. Appl. Phys. **36**, 4695 (1997), and references therein.
[16] R. W. Boswell and F. F. Chen, IEEE Trans. Plasma Sci. **25**, 1229 (1997), and references therein.
[17] F. F. Chen and R. W. Boswell, IEEE Trans. Plasma Sci. **25**, 1245 (1997), and references therein.
[18] F. F. Chen, Plasma Phys. Controlled Fusion **33**, 339 (1991).
[19] S. Shinohara, S. Takechi, and Y. Kawai, Jpn. J. Appl. Phys. **35**, 4503 (1996).
[20] S. Shinohara, S. Takechi, N. Kaneda, and Y. Kawai, Plasma Phys. Controlled Fusion **39**, 1479 (1997).
[21] S. Takechi, S. Shinohara, and Y. Kawai, Jpn. J. Appl. Phys. **36**, 4558 (1997).
[22] F. R. Chang-Díaz, Trans. Fusion Technol. **35**, 87 (1999).
[23] N. Attico, F. Califano, and F. Pegoraro, Phys. Plasmas **7**, 2381 (2000).

[24]D. Biskamp, E. Schwarz, and J. F. Drake, Phys. Rev. Lett. **76**, 1264 (1996).
[25]A. S. Kinsep, K. V. Chukbar, and V. V. Yan'kov, in *Reviews of Plasma Physics* (Consultants Bureau, New York, 1990), Vol. 16.
[26]S. Takechi, S. Shinohara, and Y. Kawai, Surf. Coat. Technol. **112**, 15 (1999).
[27]S. Takechi, S. Shinohara, and A. Fukuyama, Jpn. J. Appl. Phys. **38**, 3716 (1999).
[28]S. Takechi and S. Shinohara, Jpn. J. Appl. Phys., Part 2 **38**, L1278 (1999).
[29]A. Fukuyama and Y. Ichida, in *Proceedings of the 1996 International Conference on Plasma Physics, Nagoya, 1996*, edited by H. Sugai and T. Hayashi (The Japan Society of Plasma Science and Nuclear Fusion Research, Nagoya, 1997), Vol. 2, p. 1342.
[30]S. S. Sazhin, Astrophys. Space Sci. **158**, 107 (1989).
[31]S. S. Sazhin, Planet. Space Sci. **38**, 327 (1990).
[32]R. K. Fisher and R. W. Gould, Phys. Fluids **14**, 857 (1971).